http://dx.doi.org/10.5012/bkcs.2014.35.1.257

Notes

Ordered Mesoporous Carbon-MoO_2 Nanocomposite as High Performance Anode Material in Lithium Ion Batteries

Yuanyuan Zhou, Ilbok Lee,† Chul Wee Lee, Han Soo Park,† Hyungbin Son,†,* and Songhun Yoon†,*

Green Chemical Technology Division, Korea Research Institute of Chemical Technology (KRICT) & University of Science and Technology (UST), Daejeon 305-600, Korea
†School of Integrative Engineering, Chung-Ang University, Seoul 156-756, Korea
**E-mail: being@cau.ac.kr (H. S), yoonshun@cau.ac.kr (S. Y)*
Received August 21, 2013, Accepted October 1, 2013

Key Words : Oxide, Ordered mesoporous carbon, Anode, Lithium ion batteries

Recently, many efforts have been made in order to develop advanced anode materials in lithium ion batteries (LIBs). Particularly, transition-metal oxides, such as TiO_2, Fe_2O_3, CoO and WO_{3-x}, have been intensively investigated as promising anode candidates for LIBs. It has been reported that such materials have the merits as anodes in LIB, such as cheap material cost, high capacity and high material density.[1] Because of intrinsically low electric conductivity of these metal oxides, however, nanocomposite formation with carbon has been tried in order to provide better electrical pathway through carbon phase.[2,17,19,20] Especially, nanocomposites between transient metal oxides and ordered mesoporous carbon (OMC) have become more attractive due to their beneficial characteristics: i) abundant lithium storage sites and fast lithium diffusion in nanosized metal oxides and OMC; ii) facile electrolyte penetration owing to ordered mesopores iii) higher electric conductivity through carbon framework.[2,17,19,20]

As a novel metal-oxide anode candidate, molybdenum oxides (MoO_x, x = 2-3), which possess a theoretical specific capacity of 840-1100 mAh g^{-1} based on the mechanism of conversion reaction, have attracted considerable interest as anode material materials in LIBs.[3,4] However, it has been elucidated that in bulk MoO_x electrodes, only addition-type lithium storage reaction happens rather than conversion reaction, which leads to quite limited specific capacity and their intrinsically low electric and ionic conductivity retards their rate performance.[4,5] Accordingly, nanostructured MoO_x anodes of various forms (nanobelts, nanorods and nanoporous structures) have been prepared and great improvement has been observed.[4-6] Particularly, the ordered mesoporous MoO_2 templated from the KIT-6 silica has been reported, which exhibited largely enhanced anode performance.[5] Nevertheless, the employed preparation was based on the high-cost and environmentally unfriendly hard templating method, which required multi-step procedures including the hazardous hydrofluoric acid etching. Furthermore, a mesoporous carbon-MoO_2 nanocomposite has been recently prepared by the traditional post-addition method.[7] Although better electrochemical performance was observed, this preparative method was still tedious and more importantly, the post-added metal precursors were difficult to be localized in the inner pores during a high-temperature calcination, which resulted in crystal aggregation and relatively inhomogeneous dispersion of MoO_2 within the OMC matrix.[7]

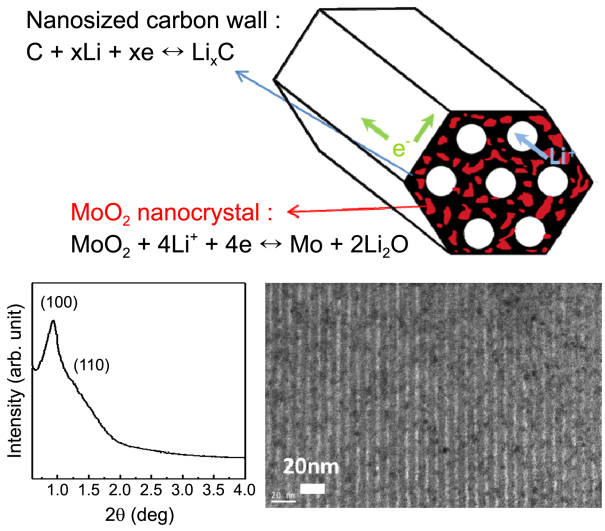

Figure 1. Schematic explanation of the ordered mesoporous MoO_2-carbon nanocomposite showing advantageous features for anode material in lithium ion batteries.

Triconstituent co-assembly, which utilizes the strong molecular interaction between carbon precursor, inorganic precursor and surfactants, has been recognized as an attractive strategy to prepare the OMC/various transient metal oxide composites within one step.[8] In our previous work, triconstituent co-assembly method has been successfully employed to prepare OMC/MoO_2 nanocomposite, namely triconstituent ordered mesoporous carbon-MoO_2 nanocomposites

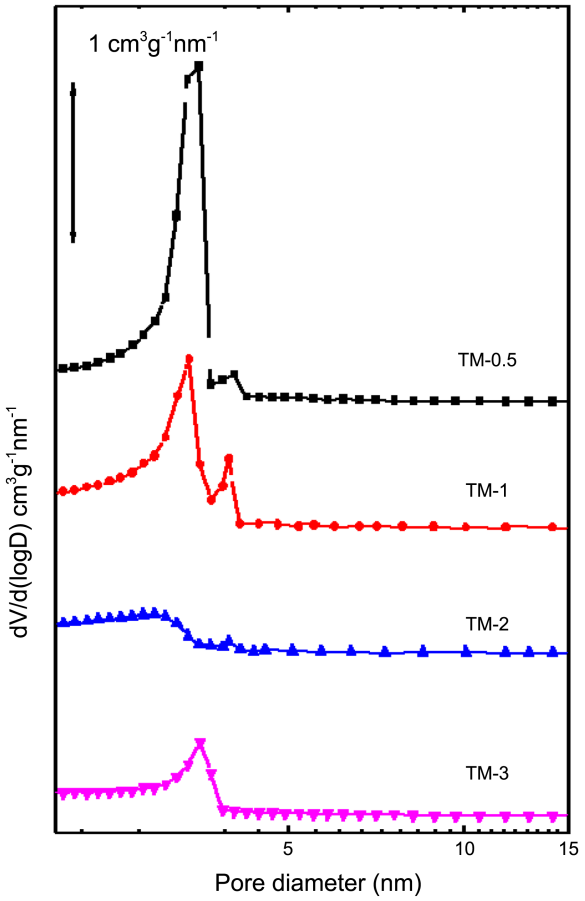

Figure 2. The pore size distribution of TM series calculated by the Barrett-Joyner-Halenda method based on the experimental N_2 sorption isotherms.[16]

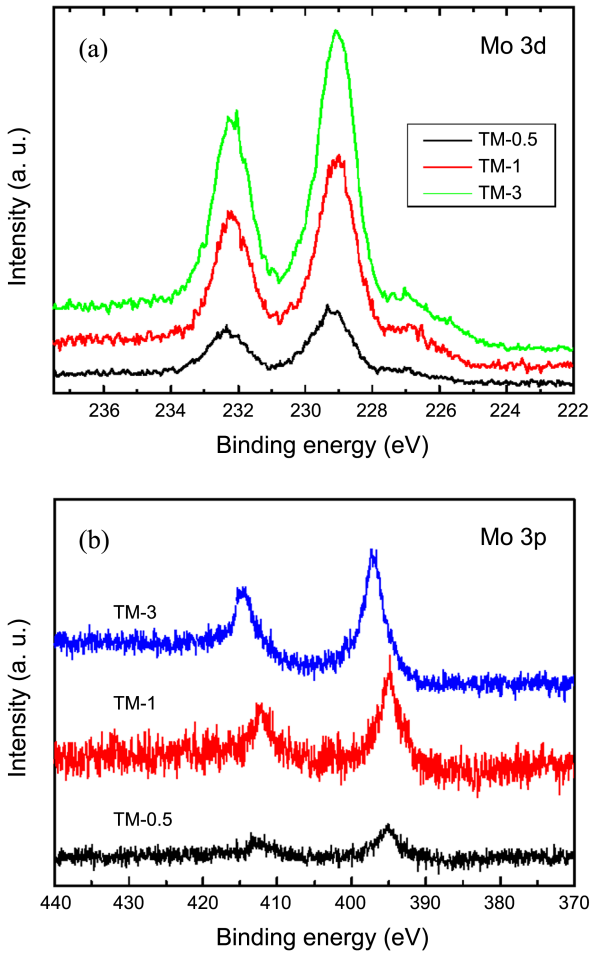

Figure 3. XPS spectra of TM series (a) Mo 3d spectra and (b) Mo 3p spectra.

(TMs).[16] However, their anode performance in lithium ion batteries remains unknown. To the best of our knowledge, this is the first report on the one-step etching-free synthesis of ordered mesoporous carbon-MoO_2 nanocomposite for the application to anode materials in lithium ion batteries.

Figure 1 schematically demonstrated the merits of the prepared TM materials with a hexagonally ordered mesoporous structure as LIB anodes. As seen, two lithium-storage sites, carbon and MoO_2, exist together in the TM materials. It is expected that the mesoporous structure provides the high electrolyte penetration through the tubular-like nanopores and short lithium diffusion paths within the nanosized wall, and meanwhile the carbon wall functions as a conductive framework.[2,17,19,20] As listed in Table 1, adsorbed N_2 volume became gradually smaller with an increase of MoO_2 fraction, which resulted in the decrease of measured BET surface areas from 640 to 381 $m^2 g^{-1}$. The pore size distributions (PSDs) for TM series were estimated from the BJH method, which are displayed in the Figure 2. A monodispersed PSD was obtained in TM-0.5 materials with a diameter of 3.4 nm, which was similar to soft-templated OMCs with F127 as the structure-directing agent.[2,9,10] However, broadening of PSD was observed in an accordance with an increase of MoO_2 fraction, although similar pore sizes were observed. This indicated that a possible structural collapse occurred for addition of more Mo precursors, which was confirmed by the XRD and TEM analysis later. As shown in Figure 1, the small-angle XRD patterns, one distinctive peak (100) near to $2\theta = 1.0^o$ and one shoulder peak (110) near to $2\theta = 1.5^o$ were observed in TM-0.5, implying a hexagonal pore packing (space group of *P*6*mm*) with lattice parameter of about 9 nm.[7,10] Similar diffraction peaks were exhibited for other TM samples while the peak intensity was gradually decreased and even only one shoulder peak appeared for TM-3.[16] Such changes were caused by two possible reasons: i) mesostructure collapse happened; ii) more crystalline MoO_2 phases adsorbed X-ray which decreased the relative contrast between pores and amorphous carbon.

In Figure 3, X-ray photoelectron spectroscopy experiment has been conducted in order to determine the Mo oxidation states. As shown in Figure 3(a), Mo 3d spectra, typically consisted of two envelopes (Mo $3d_{5/2}$ and Mo $3d_{3/2}$), are employed to estimate the distribution of Mo oxidation states. In the Mo 3d spectra, well-resolved doublet with little defect for Mo $3d_{5/2}$ at 229.1 eV and Mo $3d_{3/2}$ 232.3 eV can be easily assigned to Mo^{4+}.[2,11,21] Note that the negligible defect site at around 227 eV is attributed to either the intermediate between Mo^{4+} and Mo^0 or Mo^0.[21] Also, Figure 3(b) displayed

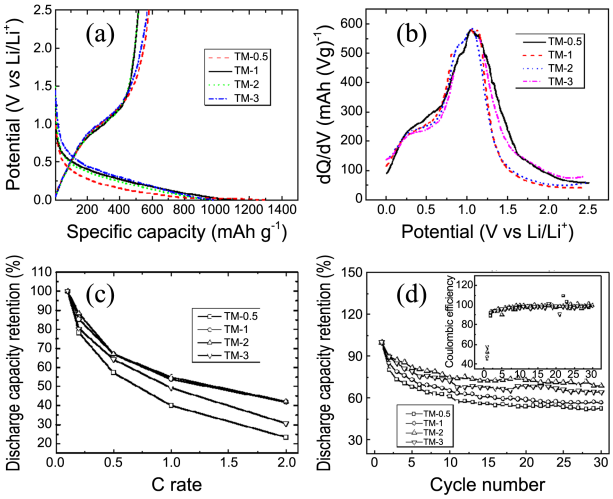

Figure 4. (a) Galvanostatic charge-discharge profiles of TM electrodes; (b) Differential discharge capacity per voltage patterns derived from the galvanostatic charge-discharge profiles; (c) Rate capability comparison between TM electrodes; (d) Cycle life and Coulombic efficiency comparison (up to 30 cycles) between TM series.

that the Mo 3p doublet spectra with Mo $3p_{1/2}$ peak at around 394.8 eV and Mo $3p_{3/2}$ peak at around 413.5 eV further confirms the presence of MoO_2 in the nanocomposites.[11,18] The reduction to Mo^{4+} was possibly attributed to the use of reductive ethanol solvent and/or the high-temperature calcination confined reductive carbon phase.[12,17] Because XPS signal was obtained within material surface, therefore, blue shift in Mo 3p spectra according to decrease of the Mo fraction indicated that Mo species located on the surface became more labile to be exposed by reducing atmosphere. Also, one can expect that electrical conductivity became higher due to higher reduction state of Mo. However, the influence of more reduced Mo species on electrical conductivity is expected to be less effective due to highly conductive carbon framework considering the large fraction of conductive carbon phase (above 60 wt %) as listed in Table 1.

Figure 4(a) displays the galvanostatic charge-discharge profiles of the TM electrodes. Because both OMC and MoO_2 are electrochemically active for Li^+ storage, their contributions to the anode capacity should be considered jointly. In OMC materials, it is well-known that Li^+ storage capacity is proportional to the surface area and the pore structures.[14] In the literature, the OMC electrodes that was prepared by a very similar method to our TM materials exhibited a discharge capacity varied between 300 and 1000 mAh g^{-1}, which was highly dependent on the surface area (650 and 2390 m^2 g^{-1}, respectively).[13,14] As listed in Table 1, the discharge capacity (C_{dis}) of TM-0.5, −1, −2 and −3 electrodes was 581, 512, 514 and 571 mAh g^{-1}, respectively, in spite of the low surface area (640-381 m^2 g^{-1}). For TM-1 and 2 anodes, decrease of C_{dis} was probably due to co-effect originated from reduction of Li^+ storage sites within carbon induced by the surface area decrease and capacity rise in TM-3 was attributed to MoO_2 fraction increase. In addition,

Table 1. Physical properties and anode performance of TM materials

	TM-0.5	TM-1	TM-2	TM-3
x_{carbon} (wt %)	91	83	71	62
x_{MoO2} (wt %)[a]	9	17	29	38
A_{BET} (m^2g^{-1})[b]	640	589	424	381
V_{ads} (cm^3g^{-1})[c]	0.37	0.32	0.22	0.21
C_{dis} (mAh g^{-1})[d]	581	512	514	571
IE (%)[e]	45	47	52	57
Rate (%)[f]	23.4	41.9	42.1	30.6
Cycle (%) [g]	52.5	56.6	68.7	64.1

[a]weight fraction of carbon and MoO_2 obtained by ICP method. [b]BET surface area. [c]adsorbed N_2 volume from N_2 sorption analysis. [d]reversible capacity of anode materials. [e]initial efficiency at first charge-discharge. [f]rate capability measured by capacity ratio between 0.1 C and 2 C rate. [g]capacity retention at 30 cycle.

the initial efficiency (IE) of OMC anodes remained almost constant (approximately 30%) irrespective of the OMC preparation methods.[2,13,14] The IE of our TM materials (45-57%) was higher than the pure OMC, which should be related with the embedded MoO_2 nanophases. As listed in Table 1, increase of IE was attributed to decrease of surface area and increase of MoO_2 fraction because electrolyte decomposition on carbon surface can be major irreversible reaction during initial charging. In addition, it is highly probable that the irreversible oxygen reaction during conversion reaction of MoO_2 can contribute the observed low IE of TM electrodes. However, this irreversible reaction can be a smaller contribution in total IE than other two factors because IE became larger according to increase of MoO_2 amount as listed in Table 1.

Note that discharge capacity contribution by MoO_2 itself for TM-3 anode was estimated to be above 900 mAh g^{-1} under assumption of 300 mAh g^{-1} C_{dis} of carbon, indicative of conversion based full Li^+ uptake (838 mAh g^{-1} for 4 Li^+) in MoO_2 nanocrystals (see equation in Fig. 1).[15] In Figure 4(b), differential discharge capacity patterns are plotted, which demonstrates that the conversion reaction by MoO_2 near 1.2 V *vs.* Li/Li^+ was dominantly observed in TM electrodes, indicative of low overpotential (0.4 V) from theoretical reaction voltage (1.6 V *vs.* Li/Li^+).[4,5,12] This further supports the conversion reaction in the MoO_2 nanoparticle embedded within carbon walls in TM materials. As shown in Figure 4(c), high rate capability (43% capacity retention at 2C current rate) was observed in TM-1 and 2 electrodes while the other two electrodes exhibited relatively low rate capability. This is attributed to optimized Li^+ transport in the pore wall and fast electrolyte transport within highly ordered mesopores in TM-1 and 2 electrodes. When compared with conventional MoO_2 electrodes which showed sluggish conversion reaction, our TM electrodes exhibited a highly advanced rate capability.[7] However, the gradual capacity decrease in every electrode was observed in Figure 4(d) and Table 1, which was mostly ascribed to the characteristic capacity decay in the ordered mesoporous carbon electrode.[11] The cycle performance of TM-2 exhibited the best result, which

was probably due to highly stabilized structure by optimized interaction between MoO_2 and carbon framework. In addition, as shown in the inset figure of Figure 4(d), the Coulombic efficiency of all the TM anodes quickly ramped to nearly 100% after initial cycle, indicative of no further irreversible consumption of Li^+. To sum up, the improved anode performance in TM materials was ascribed to complete nanocomposite formation between MoO_2 and carbon with high mesoporosity remained.

In conclusion, the ordered mesoporous carbon-MoO_2 nanocomposites were synthesized based on tri-constituent co-assembly using $MoCl_5$, resols and a commercial tri-block co-polymer F127. Low-crystallinity MoO_2 nanophases have been successfully confined within pore walls of the ordered mesoporous carbon matrix. As novel anode materials, enhanced capacity, better initial efficiency and improved rate capability were observed in the composite materials, due to the beneficial effect of high electrical conductivity, short Li^+ diffusion length and high electrolyte transport.

Experimental

Preparation of TM materials has been reported in our previous work.[16] Briefly, self-made oligomeric resols, a cheap $MoCl_5$ and the commercialized surfactant (Pluronic® F127) were utilized to introduce an evaporation-induced self-assembly (EISA) reaction. With $MoCl_5$ reacting with the solvent ethanol, Mo=O bond forms, which enables the formation of hydrogen bonds between Mo-containing compound and the hydroxyl groups (-OH) of resols and the hydrophilic parts of F127.[9,10] The initial green color of $MoCl_5$ ethanol solution was turned into brown during the reaction with resols which was then converted to black after evaporation, reflecting the strong interaction between the reactant molecules.[8,9] After calcination in an inert atmosphere at 600 °C, TMs, were obtained. Initially, 0.137 g (0.5 mmol), 0.273 g (1 mmol), 0.546 g (2 mmol) and 0.820 g (3 mmol) of $MoCl_5$ was reacted with 1 g of resol and 1.6 g of F127, and the corresponding samples were denoted as TM-0.5, TM-1, TM-2 and TM-3, respectively. The weight fraction of MoO_2 of the TM samples was determined by inductively coupled plasma (ICP) mass spectroscopy.

For the preparation of composite anodes, TM materials were mixed with a conducting agent (Super P) and polyvinylidene difluoride (PVDF) binder with a weight ratio of 8:1:1. The mixture was then dispersed in *N*-methylpyrrolidone (NMP) and spread on Cu foil (apparent areas of 1 cm^2), followed by pressing and drying at 120 °C for 12 h. Typical electrode loading and thickness was about 1.5 mg cm^{-2} and 50 μm, respectively. The half-cell characteristics were analyzed with a coin-type (CR2016) two-electrode cell in which lithium foil (Cyprus Co.) was used. The electrolyte was 1.0 M $LiPF_6$ in 1:1 (v/v) ethylene carbonate (EC)/dimethyl carbonate (DMC) (Tomiyama Co.). To investigate the anode performance in a LIB, galvanostatic charge–discharge testing in a voltage range of 2.5 to 0 V *vs*. Li/Li^+ was conducted. For the rate performance measurement, the current was varied from 0.1 to 2 C. The cycle performance for 30 cycles was recorded at a 0.1 C rate. All of the electrochemical measurements were conducted using a WBCS-3000 battery cycler (WonATech Co.)

Acknowledgments. This research was supported by KRICT and Chung-Ang University Research Grants in 2013.

References

1. Poizot, P.; Laruelle, S.; Grugeon, S.; Dupont, L.; Tarascon, J.-M. *Nature* **2000**, *407*, 496.
2. Zhou, Y.; Kim, Y.; Jo, C.; Lee, J.; Lee, C. W.; Yoon, S. *Chem. Commun.* **2011**, *47*, 4944.
3. Lou, X. W.; Zeng, H. C. *J. Am. Chem. Soc.* **2003**, *125*, 2697.
4. Sun, Y.; Hu, X.; Yu, J. C.; Li, Q.; Yuan, L.; Zhang, W.; Huang, Y. *Energy Environ. Sci.* **2011**, *4*, 2870.
5. Shi, Y.; Guo, B.; Corr, S. A.; Hu, Y.-S.; Heier, K. R.; Chen, L.; Seshadri, R.; Stucky, G. D. *Nano Lett.* **2009**, *9*, 4215.
6. Brezesinski, T.; Wang, J.; Tolbert, S. H.; Dunn, B. *Nat. Mater.* **2010**, *9*, 146.
7. Zhou, Y.; Lee, C. W.; Yoon, S. *Electrochem. Solid-State Lett.* **2011**, *14*(10), 1.
8. Liu, R.; Ren, Y.; Shi, Y.; Zhang, F.; Zhang, L.; Tu, B.; Zhao, D. Y. *Chem. Mater.* **2008**, *20*, 1140-1146.
9. Liu, R.; Shi, Y.; Wan, Y.; Meng, Y.; Zhang, F.; Gu, D.; Chen, Z.; Tu, B.; Zhao, D. *J. Am. Chem. Soc.* **2006**, *128*, 11652.
10. Limberg, C.; Boese R.; Schiemenz B. *J. Chem. Soc., Dalton Trans.* **1997**, 1633.
11. Choi, J.-G.; Thompson L. T. *Appl. Surf. Sci.* **1996**, *93*, 143.
12. Ozkan, E.; Lee, S.-H.; Liu, P.; Tracy, C. E.; Tepehan, F. Z.; Pitts, J. R.; Deb, S. K. *Solid State Ionics* **2002**, *149*, 139.
13. Zhou, H.; Zhu, S.; Hibino, M.; Honma, I.; Ichihara, M. *Adv. Mater.* **2003**, *15*, 2107.
14. Li, H.-Q.; Liu, R.-L.; Zhao, D. Y.; Xia, Y.-Y. *Carbon* **2007**, *45*(13), 2628.
15. Ku, J. H.; Jung, Y. S.; Lee, K. T.; Kim, C. H.; Oh, S. M. *J. Electrochem. Soc.* **2009**, *156*(8), A688.
16. Zhou, Y.; Lee, C. W.; Kim, S.-K.; Yoon, S. *ECS Electrochem. Lett.* **2012**, *1*, A17.
17. Jo, C.; Hwang, J.; Song, H.; Dao, A. H.; Kim, Y.-T.; Lee, S. H.; Hong, S. W.; Yoon, S.; Lee, J. *Adv. Funct. Mater.* **2013**, *23*, 3747.
18. Katrib, A.; Sobczak, J. W.; Krawczyk, M.; Zommer, L.; Benadda, A.; Jablonski, A.; Maire, G. *Surf. Interface Anal.* **2002**, *34*, 225.
19. Zhou, Y.; Jo, C.; Lee, J.; Lee, C. W.; Qao, G.; Yoon, S. *Micropor. Mesopor. Mater.* **2012**, *151*, 172.
20. Zhou, Y.; Lee, J.; Lee, C. W.; Wu, M.; Yoon, S. *ChemSusChem* **2012**, *5*, 2376.
21. Naumkin, A. V.; Kraut-Vass, Anna; Gaarenstroom, S. W.; Powell, C. J. *NIST Standard Reference Database 20*, National Institute of Standards and Technology, Gaithersburg MD, 20899, http://srdata.nist.gov/xps/